ACR Oct. 1940

NATIONAL ADVISORY COMMITTEE FOR AERONAUTICS

WARTIME REPORT

ORIGINALLY ISSUED
October 1940 as
Advance Confidential Report

WIND TUNNEL TESTS OF A SUBMERGED-ENGINE FUSELAGE DESIGN

By John V. Becker and Donald D. Baals

Langley Memorial Aeronautical Laboratory
Langley Field, Va.

NACA

WASHINGTON

WIND-TUNNEL TESTS OF A SUBMERGED-ENGINE FUSELAGE DESIGN

By John V. Becker and Donald D. Baals

SUMMARY

Tests were conducted in the 8-foot high-speed wind tunnel of a 1/5-scale-model pursuit-type fuselage with a practicable internal duct arrangement designed to meet all of the air requirements of a 1000-horsepower radial engine submerged at the maximum section. Air inlet openings at the nose and outlet openings at the sides and at the tail were investigated. The internal-flow characteristics were determined and drag force and pressure-distribution data obtained.

The results showed that the required internal flow can be obtained with negligible ducting losses provided that basic principles are observed in designing the air passages. The drag increases measured with internal flow were less than the drag due to the internal losses; i.e., the effects of air inlet and outlet on the external flow were beneficial.

The over-all drag of the best arrangement tested without simulated engine resistance, but with adequate internal flow for the engine requirements at 400 miles per hour, was less than the drag of a streamline body of similar size. The maximum local-velocity increments over the noses of the models were low; therefore, the critical-compressibility speed of the fuselage would be determined by the cockpit fairing or the wing-fuselage juncture.

INTRODUCTION

The optimum pursuit-type fuselage design from an aerodynamic point of view must have a power-plant installation which does not necessitate appreciable departures from an ideally streamline form. The location of the engine in such a fuselage would be near the maximum cross section, and an extension shaft drive to a tractor or pusher propeller, or to two propellers on the wing would be necessary. In addition to the mechanical difficulties involved, lack of data on the aerodynamic characteristics of suitable air inlet and outlet openings and the question of whether adequate air flow could be maintained without large ducting losses appear to have discouraged submerged-engine designs.

Recent tests (reference 1) have shown that the external drag of a streamline fuselage with suitable nose-inlet and tail-outlet openings is no higher than that of the basic streamline body. The critical compressibility speed with these openings was as high as that of the streamline shape. The promising nature of these results prompted an extension of the investigation to include the development of a practicable internal system to operate in conjunction with the efficient openings. The general arrangement arrived at is shown in figure 1. It was the principal purpose of this investigation to study the internal flow characteristics of this design. Force and pressure-distribution data were also obtained in order to determine the external characteristics of the inlet and outlet openings tested and to corroborate the conclusions of reference 1.

SYMBOLS

V	free stream velocity
ρ_o	free stream density
q	free stream dynamic pressure, $\frac{1}{2} \rho_o V^2$
ρ	density in duct
v	mean velocity in duct
ΔH	(free stream total pressure) - (duct total pressure)
Q	volume of flow through duct, cubic feet per second
F	maximum cross-sectional area of fuselage, 0.595 sq ft
A	duct cross-sectional area
S	wetted area of duct
a	velocity of sound in air
M	Mach number V/a
R	fuselage Reynolds number, $\frac{V(\text{length of fuselage})}{\nu}$

R pressure coefficient, $(p_{local} - p_{stream})/q$.

C_{D_F} effective fuselage drag coefficient,

$$\frac{\text{(drag of combination)} - \text{(drag of wing alone)}}{qF},$$

C area coefficient for outlets, $\frac{\text{effective area}}{\text{geometric area}}$

c_f turbulent-flow skin friction coefficient,

$$\frac{\text{skin friction/sq ft}}{\frac{1}{2}\rho V^2}$$

APPARATUS AND METHODS

The NACA 8-foot high-speed wind tunnel in which the tests were carried out is a single-return, circular-section, closed-throat tunnel. The air speed is continuously controllable from about 75 to 550 miles per hour. The turbulence of the air stream as indicated by transition measurements on airfoils is unusually low but somewhat higher than in free air.

The fuselage models were supported by a 15-inch-chord airfoil of NACA 0012 section which spanned the jet (fig. 2). The relatively large interference drag of the high-wing set-up was accepted in view of the convenience of this arrangement. A fillet similar to that employed in combination No. 143 of reference 2 was used. The wing was sufficiently far removed from the various openings to preclude the possibility of measurable interference effects on the flow at the openings.

General Arrangement

The fuselages were designed around a 1000-horsepower, 48-inch-diameter engine located at the maximum section. A total-air requirement of 21,000 cubic feet per minute at rated power was assumed. At a flight speed of 400 miles per hour this quantity of flow corresponds to a flow coefficient, Q/FV, of about 0.040. The models were designed for this value of the flow coefficient.

The fuselage design investigated (fig. 1) is considered the most practicable, and the most efficient from an aerodynamic viewpoint, of several possible arrangements. A pusher propeller was assumed because of the improved propulsive efficiency possible, and the resulting simplification of the installation of an efficient air inlet opening and a forward-firing cannon. Air from the nose inlet is led on either side of the pilot's cockpit through twin expanding channels which reunite in front of the engine. A clear width of 27 inches was allowed for the pilot. Behind the engine the duct was necked down sufficiently to permit the installation of a blower necessary for ground cooling in an actual installation. Aft of the blower station the channel was divided and contracted to form two partial-annular outlet openings.

External Shape

Streamline body.- The thickness distribution up to the 24-inch station (fig. 3) was that of the modified NACA 111 streamline body (reference 1). A fineness ratio of 6.35 was used in deriving the ordinates. Behind the 24-inch station the shape of the body was governed by considerations of space requirements and propeller spinner size. The fineness ratio of the resulting streamline body is 6.79, the length being 70.95 inches and the diameter 10.44 inches.

Nose 1.- The design recommendations of reference 1 were followed in developing the lines of the noses. It was found that an inlet opening 2.80 inches in diameter (fig. 3) permitted a profile (derived from the data of reference 1) similar to that of the streamline body, a satisfactory inlet velocity ratio, and an efficient duct expansion to the area available at the pilot's station. A cockpit enclosure which faired into the developed nose profile (side view) at the 4.5-inch station was added.

Nose 2.- In designing nose 2 (fig. 4) a sacrifice in external shape was made in order to allow the use of larger internal ducts and thereby to reduce the internal losses. The profile ordinates were derived from the data of reference 1 for an inlet diameter of 3.50 inches and merge with the cockpit enclosure fairing at the 2.50-inch station.

Tails.- The outlet openings were designed for application to the basic streamline afterbody shape.

Tail 1 (figs. 3 and 5) was an annular-outlet opening of conventional design. Tail 1-a (fig. 6) was a modification of tail 1, in which the body behind the opening was undercut as recommended in reference 1 to relieve the static pressure peak occurring with the conventional outlet. Since it was shown in reference 1 that an outlet at the tail might be superior to the radial type, it was decided to include two tail outlets in this investigation even though they could obviously not be used with a pusher propeller. The external shape of tail 2 was identical with that of the streamline body (fig. 4). Tail 2-a (figs. 4 and 6) was a cusped version of tail 2, designed according to the recommendations of reference 1.

INTERNAL DUCT DESIGN

Data from references 3, 4, and 5, were applied in designing the internal flow system. The area expansions along the nose ducts (apex angles of equivalent cones), and the velocity distributions for the design flow coefficient, 0.040, are shown in figure 7 for both noses.

Nose 1.- The duct was made cylindrical for a short distance behind the inlet in an effort to avoid possible interference effects between the internal and external flows. It was then divided into two identical channels (figs. 3 and 8) which expanded uniformly at an equivalent angle of 5.8° until the 19-inch (pilot's) station was reached. At this point the mean velocity (fig. 7) had been decreased from a value of 0.56V at the inlet to about 0.19V. With the duct velocity at this low value, a less efficient expansion angle could be employed with negligible loss; an expansion of about 20° was required between the 19-inch and maximum sections. A cylindrical fairing for the engine crankcase was merged into the wall of the pilot's compartment (fig. 9).

Nose 2.- The inlet velocity for nose 2 was 0.35V, a value low enough to permit a relatively large expansion angle to be used efficiently near the inlet, due to the natural spreading of the streamlines at low inlet velocity ratios. The results of reference 5 indicated that an angle of at least 10° could be employed for about 2 inches

behind the inlet (fig. 7). The area available at the 19-inch station required a 3.7° uniform expansion from the 2-inch station, and approximately a 17° expansion to the cylindrical engine section. (See figs. 4 and 8.)

Tails 1 and 1-a.- The chief considerations in dividing and contracting the ducts leading to the annular outlets (figs. 3 and 10) were to avoid sharp bends and extended regions of high velocity. The outlet areas were calculated from estimates of the available pressure drop across the internal system for the design flow coefficient.

Tails 2 and 2-a.- The duct area at the blower station was maintained to the 55-inch station. The channel was cylindrical for 3 inches ahead of the outlets. (See figs. 4 and 10.)

Simulated engine resistance.- An orifice plate punched with 204 1/4-inch holes was employed to represent a baffled engine of conductance 0.10. An orifice coefficient of 0.70 was used in designing the plate in view of the close spacing of the holes.

Flow and Pressure Measurement

The rates of flow were measured by surveys of the total and static pressure at the blower section. A built-in rake of 5 total-pressure tubes and a ring of 4 static-pressure orifices spaced 90° apart around the duct wall were used for this purpose. Measurements of total pressure were also made at the 24.7- and 30-inch stations by inserting additional 5-tube rakes into the ducts from the outside of the model. Total-pressure traverses at the outlets were made by means of single adjustable impact tubes.

Static-pressure orifices over the top of the noses and cockpit fairings were installed to permit the estimation of critical speeds. Static pressures over the annular outlets were similarly measured to furnish additional data on the outlet characteristics.

Boundary-Layer Conditions

It has been found necessary in the 8-foot high-speed wind tunnel to fix the location of boundary-layer transi-

tion near the nose of fuselage models in order to secure results significant for high Reynolds number applications. This was accomplished by 1/4-inch-wide rings of No. 60 carborundum grains glued to the surface at the 3/4-inch station of noses 1 and 2 and at the corresponding station on the streamline nose. Aside from the carborundum strips, the surfaces of the models (both external and internal) were aerodynamically smooth and fair.

TESTS

Drag-force tests of the wing alone, of the streamline-body combination, and of a typical combination with internal flow, were carried to a Mach number of 0.67 (about 500 miles per hour). For the other combinations it was necessary only to obtain drag comparisons at a moderate speed. A value of M of 0.30 was selected from consideration of the force required for adequate precision of measurement. Actually, the tests were made at a series of speeds bracketing the desired Mach number. The force tests were made both with boundary-layer transition fixed near the nose of the models and with transition as it occurred naturally on the smooth models.

The static pressure and internal-flow measurements were made separately from the force tests because of the necessity of running the pressure tubing along the top of the wing. These tests were made at a Mach number of approximately 0.30.

Tuft survey runs were made for the streamline body (fixed transition) at speeds up to 260 miles per hour.

RESULTS

The method of computing velocity, Mach number, and Reynolds number in the 8-foot high-speed wind tunnel is described in reference 6. Compressibility effects are indicated directly since the true, rather than the indicated, dynamic pressure was used in computing the coefficients. The effective fuselage drag coefficient C_{D_F} includes the unfavorable interference of the high-wing arrangement.

The rate of internal flow is expressed nondimensionally in terms of the flow coefficient, Q/FV. The internal duct losses are shown in terms of the stream dynamic pressure because of the significance of the resulting parameter in the internal drag equation. As shown in reference 1, the internal drag coefficient depends on the flow coefficient and the total head loss as follows:

$$C_{D_F}(\text{internal}) = 2Q/FV \left[1 - (1 - \Delta H/q)^{\frac{1}{2}} \right]$$

The effect of Mach number on the drag coefficients of the streamline body and of the nose 1 - tail 1 combination is shown in figure 11. The low drag values for the natural transition condition probably could not be realized at flight Reynolds numbers owing to a rapid decrease in the extent of laminar flow as the Reynolds number is increased. For this reason it was felt not worth while to include in this report the natural transition results for the other combinations. In general, the drag increments between the natural and fixed transition conditions were almost identical with those shown in figure 11 for the nose 1 - tail 1 combination. The drag data obtained with fixed transition at a Mach number of 0.30 are given in table I together with the flow coefficients, over-all duct losses, and internal drag data for all of the combinations tested.

The results of the external static pressure measurements over the noses and annular outlets are shown in figures 12 and 13, respectively.

An analysis of the duct losses for the nose 1 - tail 1 combination and for the nose 2 - tail 2 combination is given in figures 14 and 15, respectively.

The data shown in the figures and tables are given for an angle of attack of zero degree only. No measurable fuselage drag increase was found through the test angle-of-attack range of -2° to $+3.5^\circ$.

DISCUSSION

Drag Results

Streamline body.- The tuft surveys showed excellent

flow conditions about the tail of the streamline body. Near the tail of the fillet, however, there was a region of disturbed flow. This unfavorable interference between the high wing and the body resulted in an effective drag coefficient for the body of 0.092 at the test Reynolds number of 11,200,000 (M = 0.30). The results of reference 2 for a similar model arrangement (combination 143) indicated a decrease in effective fuselage drag of 33 percent between high and midwing arrangements. Thus, a drag coefficient of about 0.060 is indicated for the streamline body if the optimum midwing arrangement were used. The interference effects at the wing fillet were local, as was demonstrated by tuft surveys, and could have no measurable influence on the characteristics of the inlet or outlet openings or the internal flow.

Critical speeds.- The pressure coefficients over the leading 4-1/2 inches of nose 1 and 2-1/2 inches of nose 2 (portions of the nose profiles derived from the shapes of reference 1) were low and the gradients favorable (fig. 12); these desirable characteristics are the same as indicated in reference 1, and the method of derivation of the profiles for a given inlet size is thus verified. It is shown in reference 1 that the critical speed of a streamline fuselage employing openings of this size and profile shape is as high as that of the basic streamline body which, for the shape tested, is estimated (reference 7) as $M_{cr} = 0.87$. The addition of cockpit fairings would reduce the critical Mach number to approximately 0.77 (estimated by the method of reference 7 from the peak pressures shown in fig. 12). The rapid increase in drag coefficient noted in the force tests at a Mach number of about 0.60 (fig. 11) for all of the combinations, is attributed to the occurrence of the compressibility burble at the wing fillet. It is evident that the critical speed of fuselages employing the nose 1 or nose 2 profiles will be fixed by some point of high local velocity other than the nose itself. The importance of careful design of the wing-fuselage juncture is also apparent.

Drag comparisons.- The cockpit fairing and the nose 1 inlet shape caused only small increases in drag above that of the streamline body (table I, arrangements 1, 2, and 3). With the internal duct open, but with no internal flow, the drag was about the same as with the duct closed at the nose (arrangement 4). In comparing the various arrangements with internal air flow (table I), account must be

taken of the drag due to the internal as well as the external flow. The external drag increment of a combination may be obtained by subtracting the internal drag increment from the over-all drag increment. It will be seen that the external drag for most of the combinations with internal flow was less than the drag of the basic streamline body. This effect results from a beneficial action of the air inlet and outlet processes on the external flow and is discussed more fully in reference 1.

Comparisons of the external drag characteristics of the openings should be made at the same value of the flow coefficient owing to a variation with flow coefficient of the interference effects between external and internal flows. Because the rate of flow varied somewhat for the various arrangements, it is possible only to make qualitative comparisons by direct use of the test data given in table I. However, the results obtained with and without the simulated engine resistance provide a means of interpolating the data to a given flow coefficient. Thus, at the design flow coefficient of 0.040 the following comparison between noses 1 and 2 as tested with tail 2-a (duct unobstructed) was obtained:

Drag increments in percent of streamline body drag

	Internal drag	External drag	Over-all drag
Nose 1	3.1	-4.5	-1.4
Nose 2	1.7	-.1	1.6

It is seen that the nose 1 arrangement is the better of the two in spite of the higher ducting losses.

The following order of merit was obtained for the four outlets in combination with nose 1, corrected to a flow coefficient of 0.040:

Outlet	External drag increment, percent
1	-0.2
1-a	-3.5
2	-1.0
2-a	-4.5

The internal drags were approximately the same for all of the outlets.

The drag increments shown above and in table I were based on the streamline body drag for the high-wing set-up (0.092). If the optimum midwing arrangement were used, the increments would be increased by about 50 percent, owing to a decrease in drag of the basic streamline body to about 0.060.

Not only was the external drag less for the modified outlets, but the rate of flow for a given outlet area was considerably increased. (Cf. arrangements 5 and 7, 8 and 9, table I.) Area coefficients showing the effectiveness of the outlets and useful for design purposes were derived as follows:

$$C = \frac{\text{effective outlet area}}{\text{geometric outlet area}} = \frac{A_{eff}}{A_1}$$

The effective area, as a fraction of the maximum section area, is given by

$$\frac{A_{eff}}{F} = \frac{Q_1}{Fv_1} \qquad \text{(Subscript } _1 \text{ refers to outlet)}$$

Since Q_1 is known, it remains to compute v_1 from Bernoulli's equation for the internal flow in order to determine A_{eff}. Assuming that free-stream total pressure is available at the inlet, that the density at the outlet is decreased due to the addition of heat, and neglecting second-order effects,

$$v_1 = \left(\frac{\rho_o}{\rho_1}\right)^{\frac{1}{2}} V \left(1 - \frac{\Delta H_1}{q} - P_1\right)^{\frac{1}{2}}$$

in which P_1 is the pressure coefficient obtaining at the outlet station with the opening faired over. Then the effective area is

$$\frac{A_e}{F} = \frac{Q_1}{FV} \left(\frac{\rho_1}{\rho_o}\right)^{\frac{1}{2}} \frac{1}{(1 - \Delta H_1/q - P_1)^{\frac{1}{2}}}$$

and

$$C = \frac{F}{A_1}\left(\frac{Q_1}{FV}\right)\left(\frac{\rho_1}{\rho_o}\right)^{\frac{1}{2}} \frac{1}{(1 - \Delta H_1/q - P_1)^{\frac{1}{2}}}$$

For design purposes the geometric outlet area may be computed from

$$\frac{A_1}{F} = \frac{1}{C}\left(\frac{\rho_1 Q_1}{\rho_o FV}\right)\left(\frac{\rho_o}{\rho_1}\right)^{\frac{1}{2}} \frac{1}{(1 - \Delta H_1/q - P_1)^{\frac{1}{2}}}$$

The last equation shows that for constant mass flow the outlet area required depends on the density ratio (i.e., on the amount of heat added to the internal flow) as well as on the available pressure drop across the internal system. The values of C obtained for the outlets tested with both noses and the values of P_1 used in their computation are as follows:

Outlet	P_1	C
1	-0.055	0.91
1-a	-.055	.93
2	.050	.84
2-a	.050	.96

These outlet coefficients, as may be seen from the method of derivation, indicate the combined effects of the shape of the openings and the interference between internal and external flows. The high values of the coefficients for the modified outlet shapes are compatible with the low external drags obtained with these shapes.

Details of the annular outlet openings and the pressure distributions obtained are shown in figure 13. It is seen that although tail 1-a resulted in a considerable improvement, further undercutting is desired to reduce the pressures to the values obtaining with the outlet faired. A further modification of the contour designed to achieve the desired result is shown.

These considerations of relative external drag, area coefficient, and pressure distribution, fully confirm the

conclusions of reference 1 regarding the optimum outlet opening shapes.

Internal-Flow Characteristics

Over-all losses.- In comparing the internal duct characteristics it should be borne in mind that the total pressure loss varies approximately as the square of the flow coefficient, and the internal drag approximately as the cube of the flow coefficient. Exact comparisons of the internal arrangements must therefore be made at a given flow coefficient. Comparing arrangements 7 and 14 (table I) which have about the same flow coefficients, it is seen that the over-all internal loss with nose 1 was about twice that with nose 2. The effect of a sharp-edged gun at the nose 1 inlet was to add about 20 percent to the internal duct losses. (Cf. arrangements 5 and 6, table I.)

It has been pointed out previously that the internal drag due to the total ducting losses at the design flow coefficient was only 3.1 percent with nose 1 and 1.7 percent with nose 2 (corresponding to over-all duct losses of 0.070 and 0.038, respectively). The magnitude of these losses may be considered negligible in comparison with the actual cooling loss, particularly in view of the appreciable decreases in external drag which accompany the internal flow.

In connection with the simulated cooling loss it should be pointed out that in these tests all of the internal air flow passed through the engine resistance whereas in an actual installation a large part of the air would be diverted to the carburetor. The internal drags shown in table I for arrangements 10, 11, 12, 16, and 17 are therefore higher than would actually be incurred at the design speed of 400 miles per hour. The pressure drop across the engine resistance in the tests corresponds to about 66 pounds per square foot at 400 miles per hour.

Analysis of losses.- The losses throughout the internal systems were computed on the basis of existing internal flow data in order to aid in analyzing the measured losses. References 3, 4, and 5 were used in estimating the bend and expansion losses. Owing to the relatively large proportion of wetted area to cross-sectional area in the designs employed, skin friction losses were an appreciable fraction of the total losses. The skin friction

losses were computed as follows by equating the summation of the local energy losses to the total energy loss:

$$\Sigma \frac{\rho}{2} v^3 c_f \, dS = Q \Delta H_{friction}$$

or

$$\frac{\Delta H}{q} \text{ (friction)} = 42.0 \; \Sigma \left(\frac{v}{V}\right)^3 c_f \, dS$$

where

$\frac{Q}{FV} = 0.040$

$\rho = \rho_o$

$\frac{v}{V}$, from figure 7

c_f, from von Kármán turbulent boundary-layer theory for the local duct Reynolds numbers

The results of the duct-loss calculations are shown in figures 14 and 15 together with the measured losses (corrected to Q/FV = 0.040). The agreement between the measured and computed total losses at the various stations is satisfactory. In general, the calculated losses are somewhat higher than the measured values. This is probably due to the fact that the bend and expansion losses, as obtained from the various references, include some friction losses. In addition, a favorable scale effect (reference 8) may have slightly reduced the measured losses.

In order to determine whether the assumption of a turbulent boundary layer was justified in computing the duct skin-friction losses, a run was made with a 1/2-inch wide strip of No. 60 carborundum around the wall of the duct 1-1/2 inches back from the nose. This modification resulted in no increase in internal loss, thus indicating that no appreciable laminar flow existed.

A study of figures 7, 14, and 15 will emphasize the importance of keeping the duct velocities low, since nearly all of the losses occurred at stations where the velocity was greater than 0.25V. Care should be taken to avoid ex-

tended regions of high velocity near the outlets. The cylindrical section ahead of the tail 2 and 2-a outlets, for example, is considered longer than necessary.

Apparently no unexpected bend or expansion losses occurred. No measurable entrance loss existed, and no flow pulsations could be detected.

The loss across the simulated engine resistance agrees well with the computed values (figs. 14 and 15) and corresponds to a conductance of 0.106 as compared with the design value of 0.100. The resistance plate caused no measurable changes in the characteristics of the internal flow near by.

The total-pressure surveys at all of the stations investigated showed that the distribution of total pressure across the channels was satisfactorily uniform. To within 1/8 inch from the walls the total pressure was never more than 0.02q different from the mean value.

CONCLUSIONS

1. The air requirements of a power plant submerged near the maximum section of a streamline fuselage can be met with negligible ducting losses provided the fundamentals of efficient duct design are followed.

2. The effect of air inlet at the nose and outlet at the tail is beneficial to the external flow. Owing to this effect, the over-all drag of the best arrangement tested without simulated engine resistance but with adequate internal flow for the 400-mile-per-hour condition was less than the drag of the basic streamline body.

3. Because of the low local velocities over the nose shapes tested, the critical compressibility speed of the fuselage would be determined by the cockpit fairing or the wing-fuselage juncture rather than by the nose shape.

4. The duct losses can be computed with sufficient accuracy for design purposes. No unexpected entrance losses or flow pulsations were apparent.

5. The conclusions of reference 1 regarding the optimum shapes of outlet openings were corroborated.

Langley Memorial Aeronautical Laboratory,
National Advisory Committee for Aeronautics,
Langley Field, Va.

REFERENCES

1. Becker, J. V.: Wind-Tunnel Tests of Air Inlet and Outlet Openings on a Streamline Body. NACA ACR, Nov. 1940.

2. Jacobs, E. N., and Ward, K. E.: Interference of Wing and Fuselage from Tests of 209 Combinations in the NACA Variable-Density Tunnel. NACA Rep. No. 540, 1935.

3. Patterson, G. N.: Modern Diffuser Design. Aircraft Engineering, vol. 10, no. 115, Sept. 1938, pp. 267-273.

4. Patterson, G. N.: Note on the Design of Corners in Duct Systems. R. & M. No. 1773, British A.R.C., 1937.

5. Patterson, G. N.: Design of Airplane Ducts. Aircraft Engineering, vol. 11, no. 125, July 1939, pp. 263-268.

6. Hood, M. J.: The Effects of Some Common Surface Irregularities on Wing Drag. NACA TN No. 695, 1939.

7. Robinson, R. G., and Wright, R. H.: Estimation of Critical Speeds of Airfoils and Streamline Bodies. NACA ACR, March 1940.

8. Klein, G. J., Tupper, K. F., and Green, J. J.: The Design of Corners in Fluid Channels. Canadian Journal of Research, vol. 3 (1930).

L-485

TABLE I

Drag and internal-flow characteristics, $M = 0.3$, $R = 11{,}200{,}000$.

Number	Model arrangement	Fuselage drag coefficient C_{D_F}	Drag increase above streamline body (percent)	Rate of internal flow Q/FV	Duct total-pressure loss $\Delta H/q$	Internal drag (percent)
1	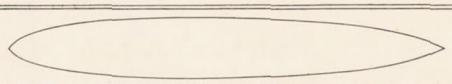	0.0918	—	—	—	—
2	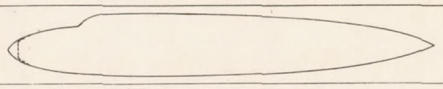	.0922	0.4	—	—	—
3	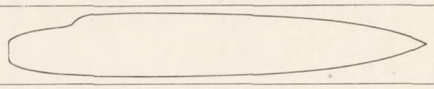	.0917	0	—	—	—
4	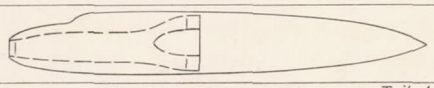	.0920	.2	—	—	—
5	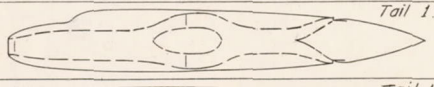 Tail 1	.0957	4.3	0.0416	0.075	3.5
6	 37 mm cannon; Tail 1	.0960	4.6	.0412	.090	4.2
7	 Tail 1-a	.0953	3.8	.0445	.085	4.3
8	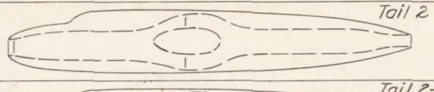 Tail 2	.0923	.5	.0348	.057	2.2
9	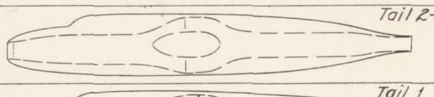 Tail 2-a	.0903	−1.6	.0394	.068	2.9
[a] 10	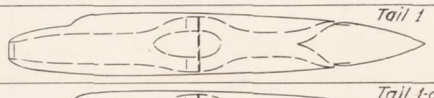 Tail 1	.0985	7.3	.0380	.202	8.9
[a] 11	 Tail 1-a	.0991	7.9	.0407	.231	11.0
[a] 12	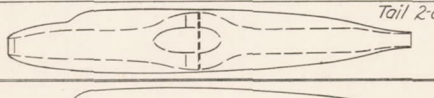 Tail 2-a	.0946	3.0	.0360	.181	7.5
13	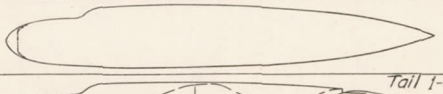	.0929	1.2	—	—	—
14	 Tail 1-a	.0955	4.0	.0451	.044	2.2
15	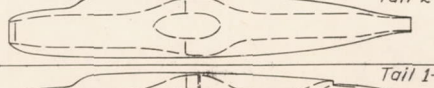 Tail 2-a	.0934	1.7	.0406	.040	1.8
[a] 16	 Tail 1-a	.0996	8.5	.0409	.192	9.1
[a] 17	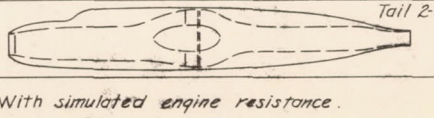 Tail 2-a	.0976	6.3	.0368	.155	6.4

Nose 1 (rows 1–12); Nose 2 (rows 13–17)

[a] With simulated engine resistance.

NACA

Fig. 1

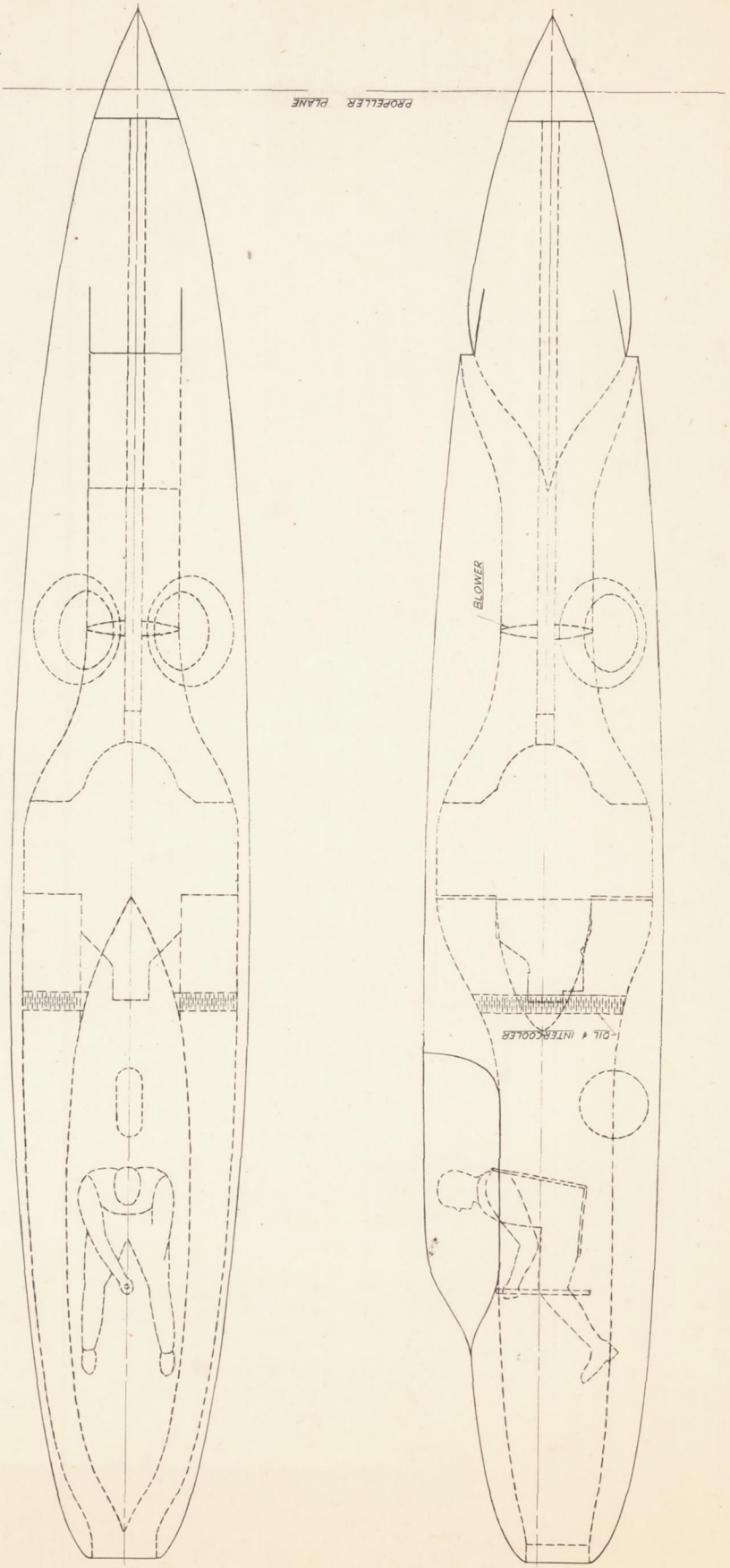

Fig. 1- General arrangement of submerged-engine fuselage.

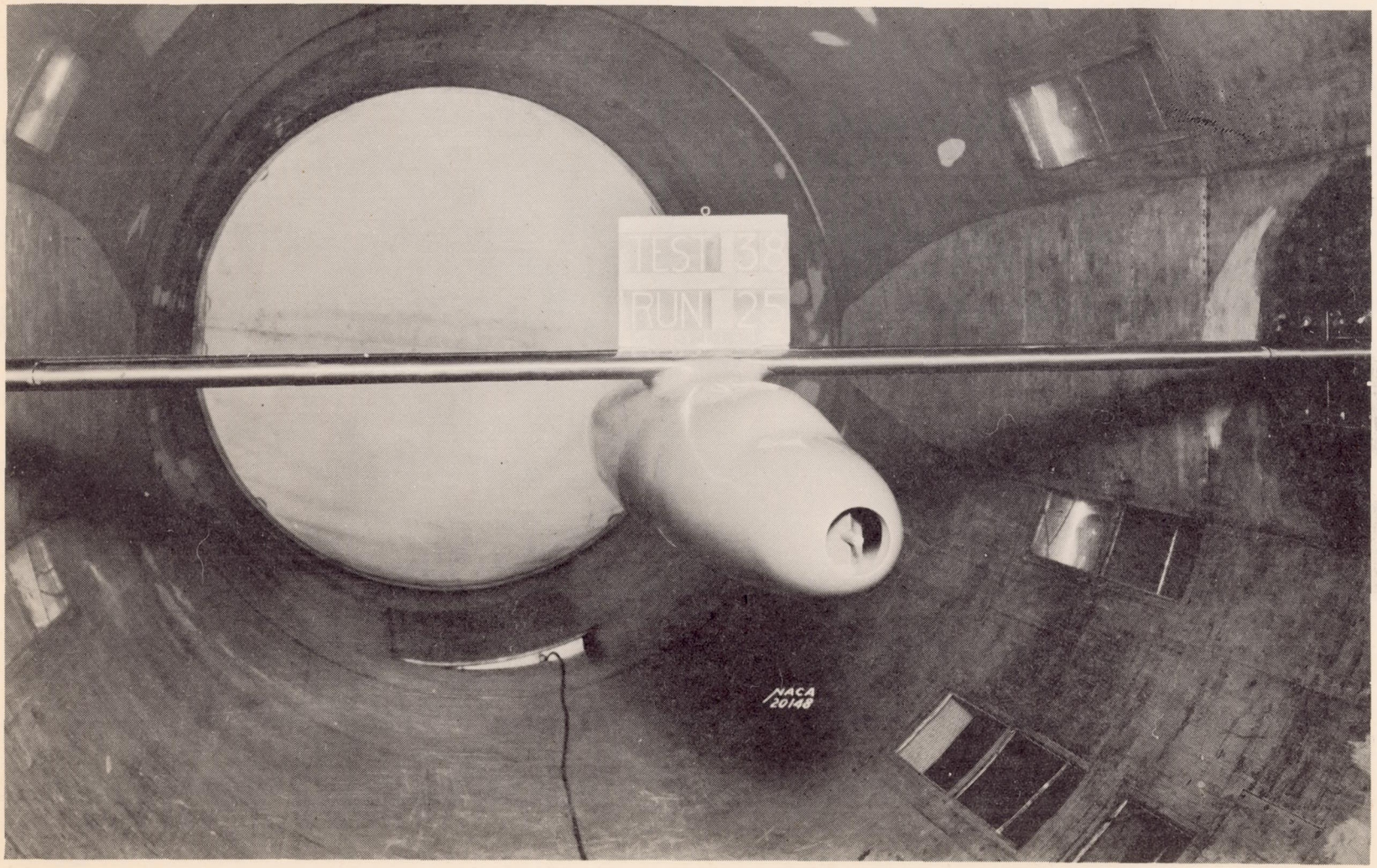

Figure 2. General view of set-up in 8-foot high speed wind tunnel.
Nose 1 with gun .

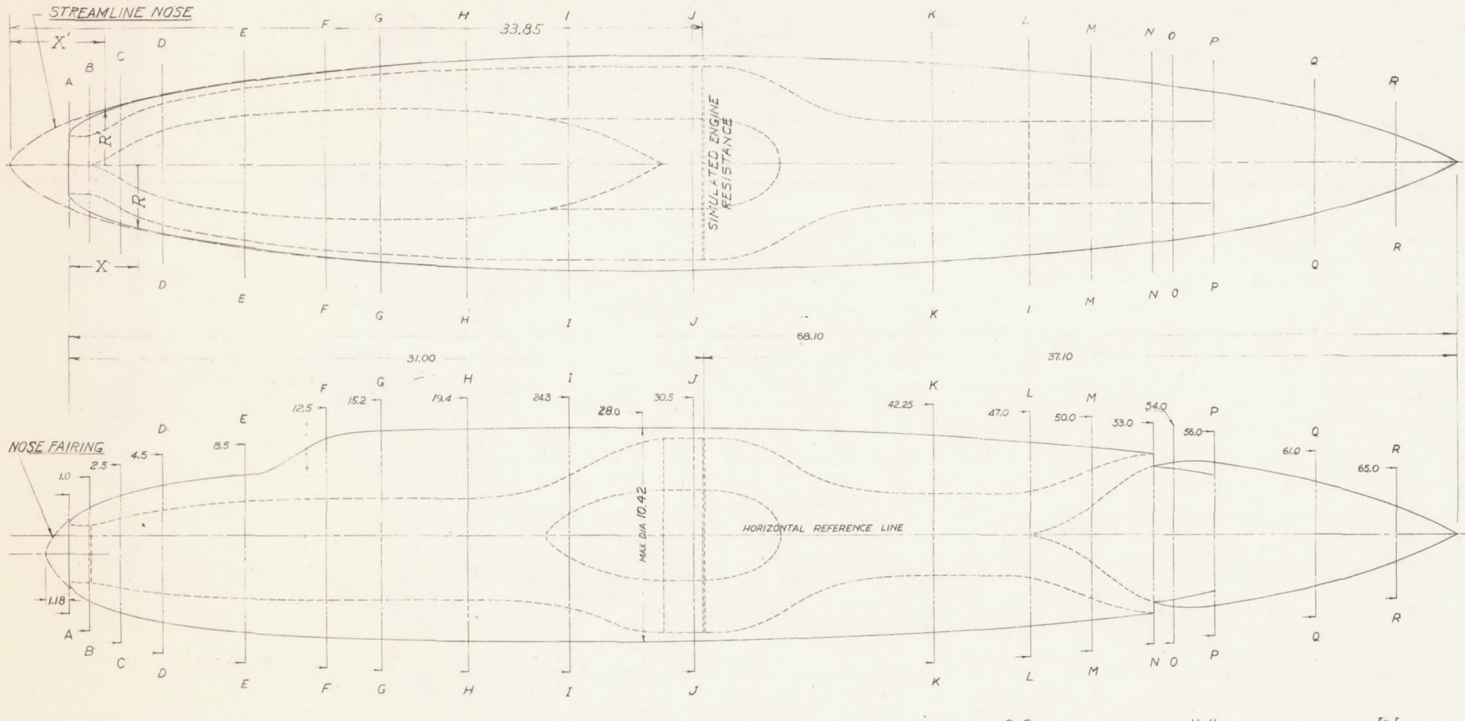

Nose Profile Ordinates	
X, inches	R, inches
0	1.45
.05	1.58
.15	1.68
.25	1.77
.50	1.97
1.00	2.26
1.50	2.48
2.00	2.68
3.00	2.99
4.00	3.23

Nose lip radius = 0.05

Streamline Nose Ordinates	
X', inches	R, inches
0	0
0.5	0.70
1.0	1.12
2.5	1.91
5.0	2.82
10.0	3.87
15.0	4.51
20.0	4.93
25.0	5.17
30.0	5.21
33.85	5.20

Duct Area	
Section	Area, sq. in.
A-A	6.16
B-B	6.60
C-C	8.24
D-D	8.32
E-E	10.40
F-F	13.08
G-G	14.80
H-H	17.84
I-I	29.28
J-J	55.60
K-K	12.56
L-L	13.50
M-M	13.20
N-N	4.03

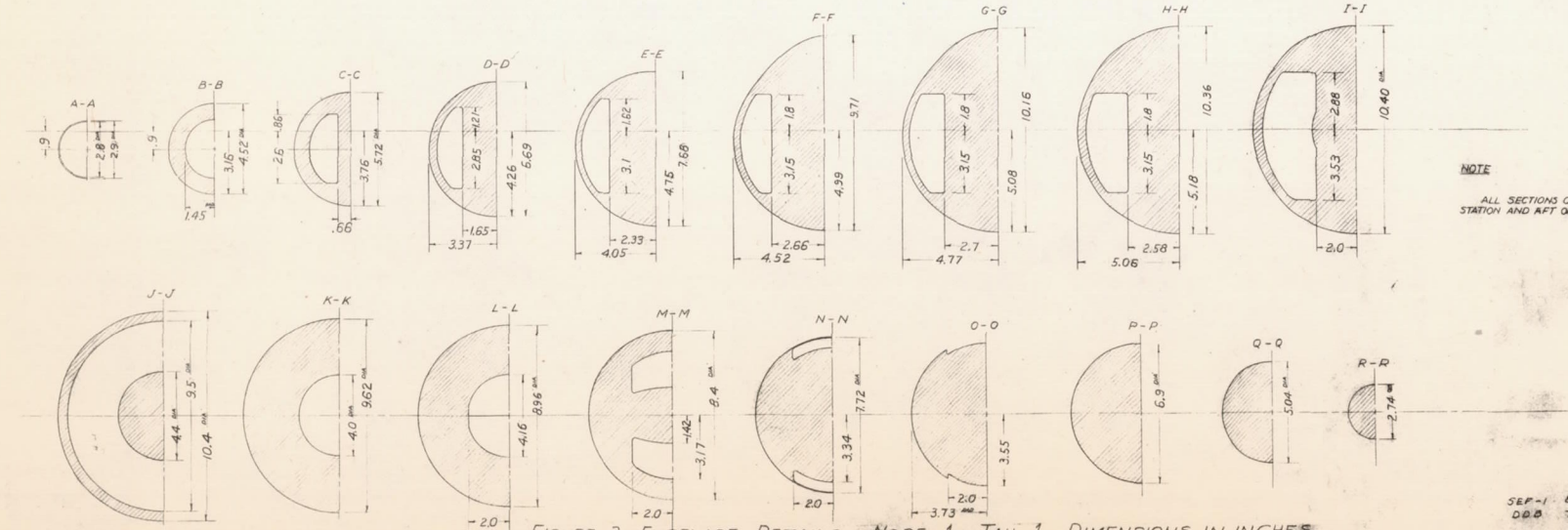

NOTE

ALL SECTIONS CIRCULAR FROM A-A TO 4" STATION AND AFT OF STATION I-I.

SEF-1 8'HST
DD.B 7-1-40

FIGURE 3.- FUSELAGE DETAILS. NOSE 1, TAIL 1. DIMENSIONS IN INCHES

Fig 3

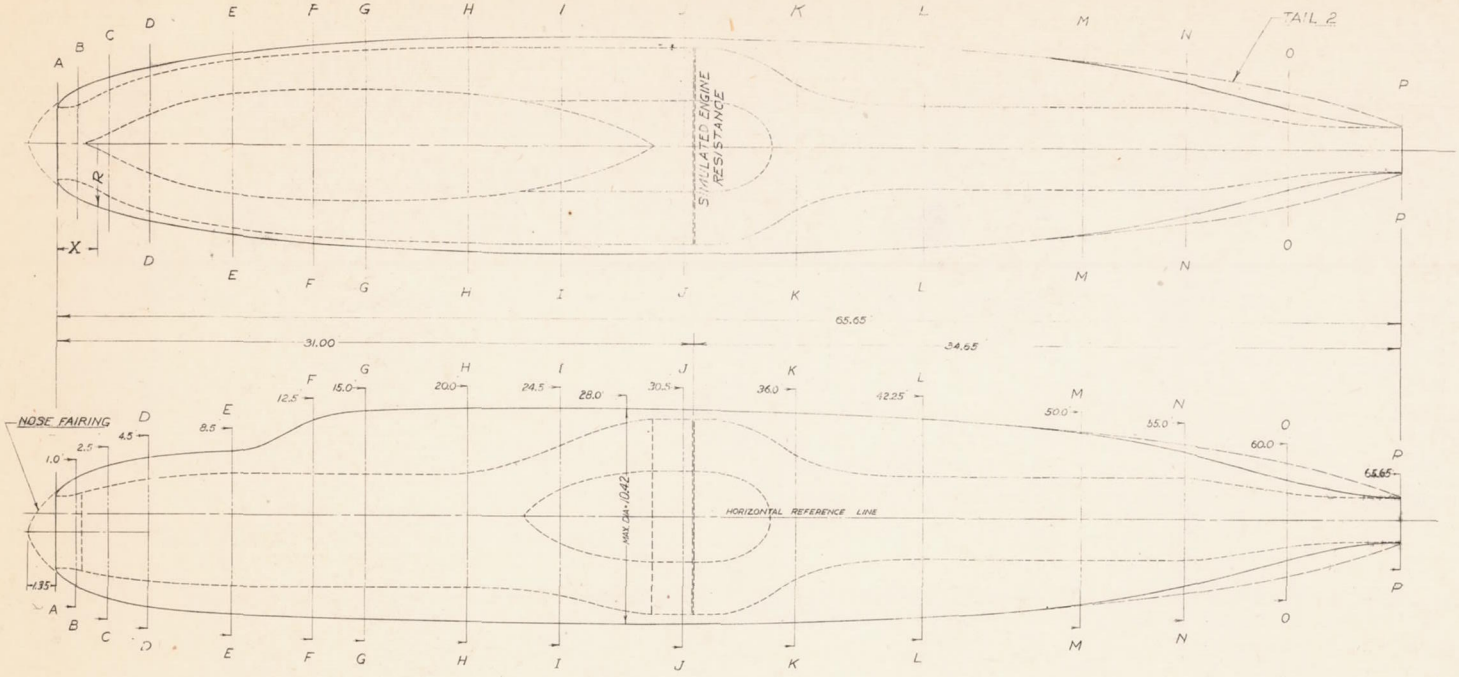

Nose Profile Ordinates	
X, inches	R, inches
0	1.80
.05	1.93
.15	2.05
.25	2.13
.50	2.32
1.00	2.61
1.50	2.85
2.00	3.05
2.50	3.22

NOSE LIP RADIUS = 0.05

Duct Area	
Section	Area, sq. in.
A-A	9.62
B-B	10.75
C-C	13.40
D-D	13.60
E-E	14.88
F-F	16.52
G-G	17.60
H-H	20.96
I-I	34.30
J-J	55.60
K-K	29.20
L-L	12.86
M-M	12.56
N-N	12.56
O-O	5.47
P-P	3.73

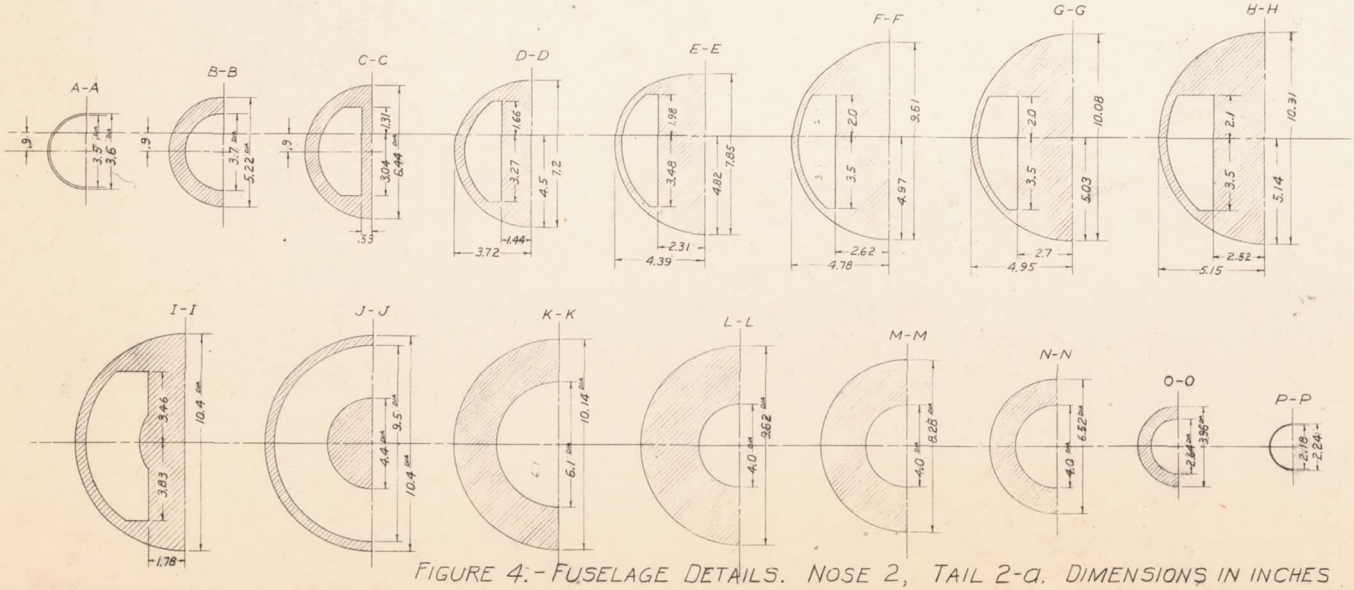

NOTE

ALL SECTIONS CIRCULAR FROM A-A TO 2.5 INCH STATION AND AFT OF STATION I-I.

TAIL 2 PROFILE ORDINATES CORRESPOND TO THOSE OF TAIL 1, FIGURE 3.

FIGURE 4.- FUSELAGE DETAILS. NOSE 2, TAIL 2-a. DIMENSIONS IN INCHES

SEF-2 B'HST
DDB 7-9-46

NACA 20617

NACA Fig. 4

NACA

Fig. 5.

Figure 5. Tail 1

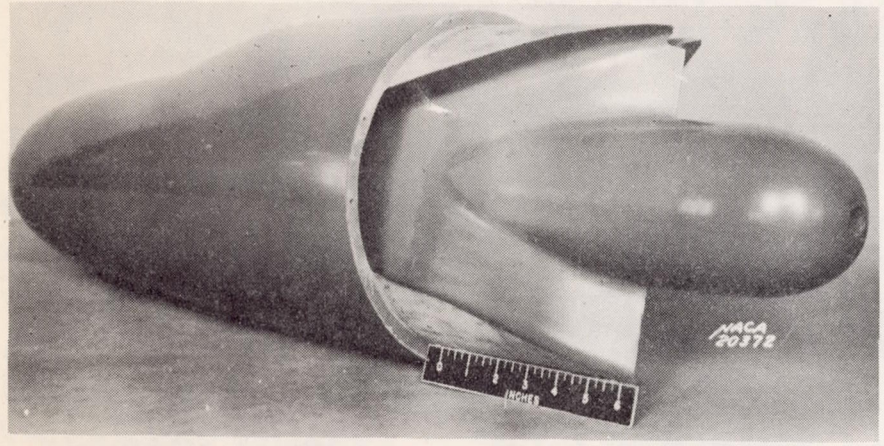

Figure 9.- Duct details showing crankcase fairing. Wall cut at 22.5-inch station. Nose 1.

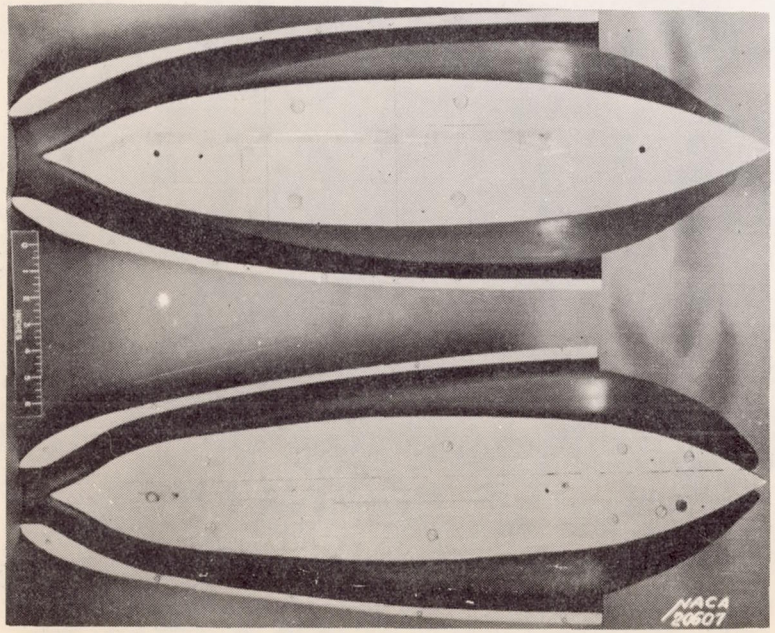

Figure 8.- Comparison of internal ducts. Nose 1 (bottom) and nose 2.

Figure 6.- Comparison of external shape of tails 1-a and 2-a.

L-485

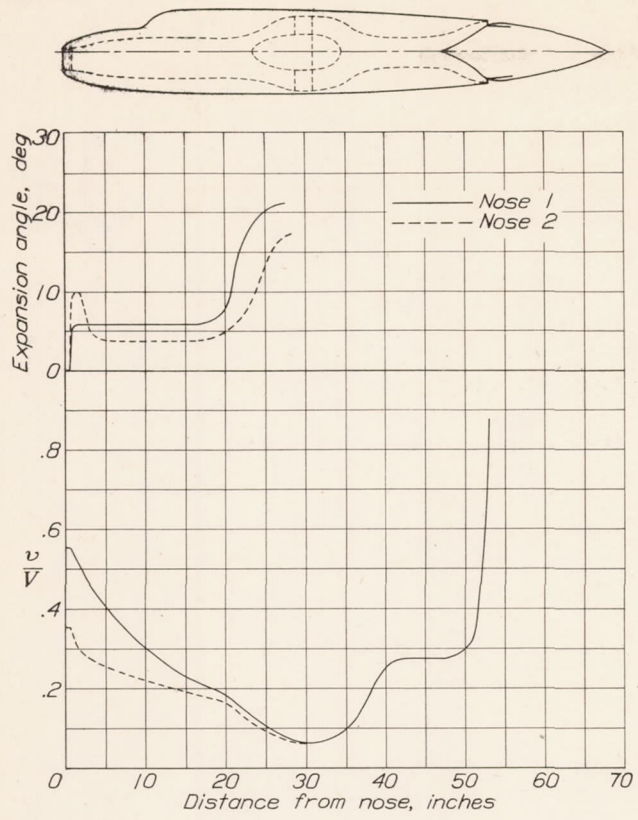

Figure 7.- Duct-velocity ratios and equivalent conical expansion angles. Q/FV=0.040.

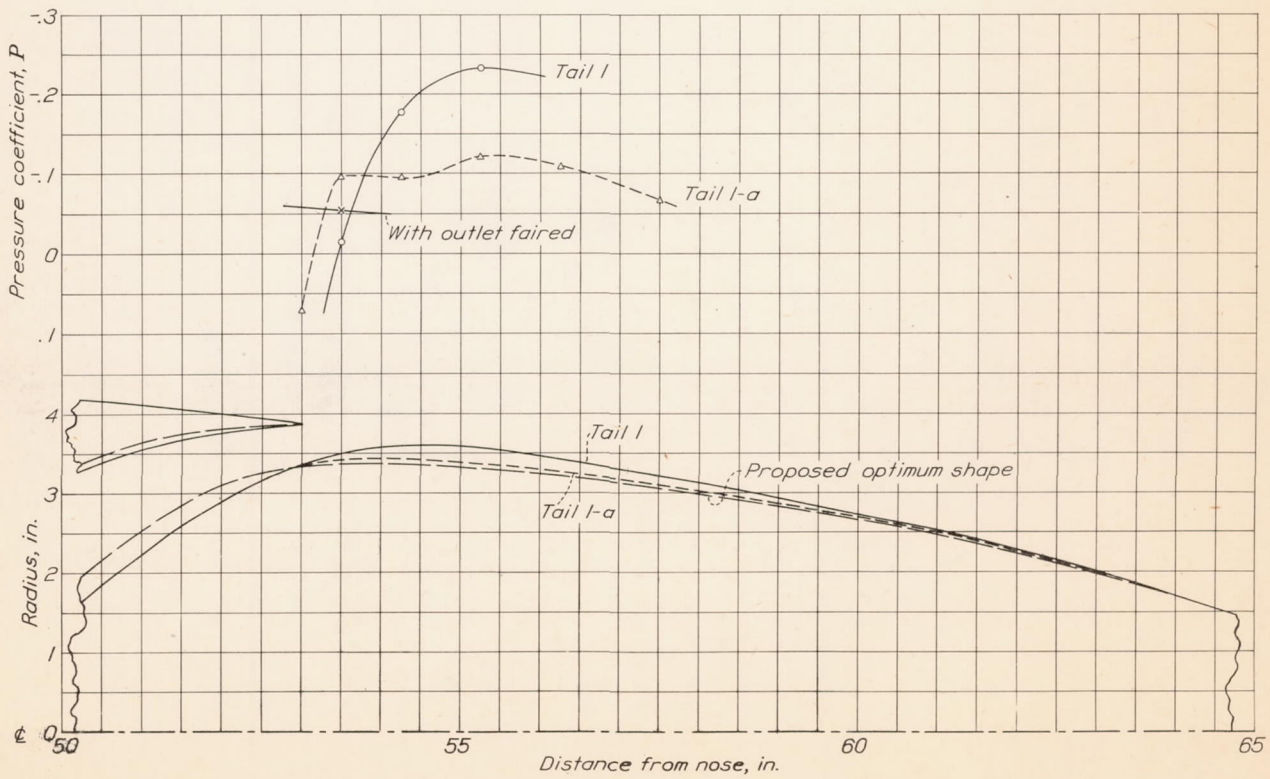

Figure 13.- Details of radial outlet openings and pressure distributions for Q/FV=0.042.

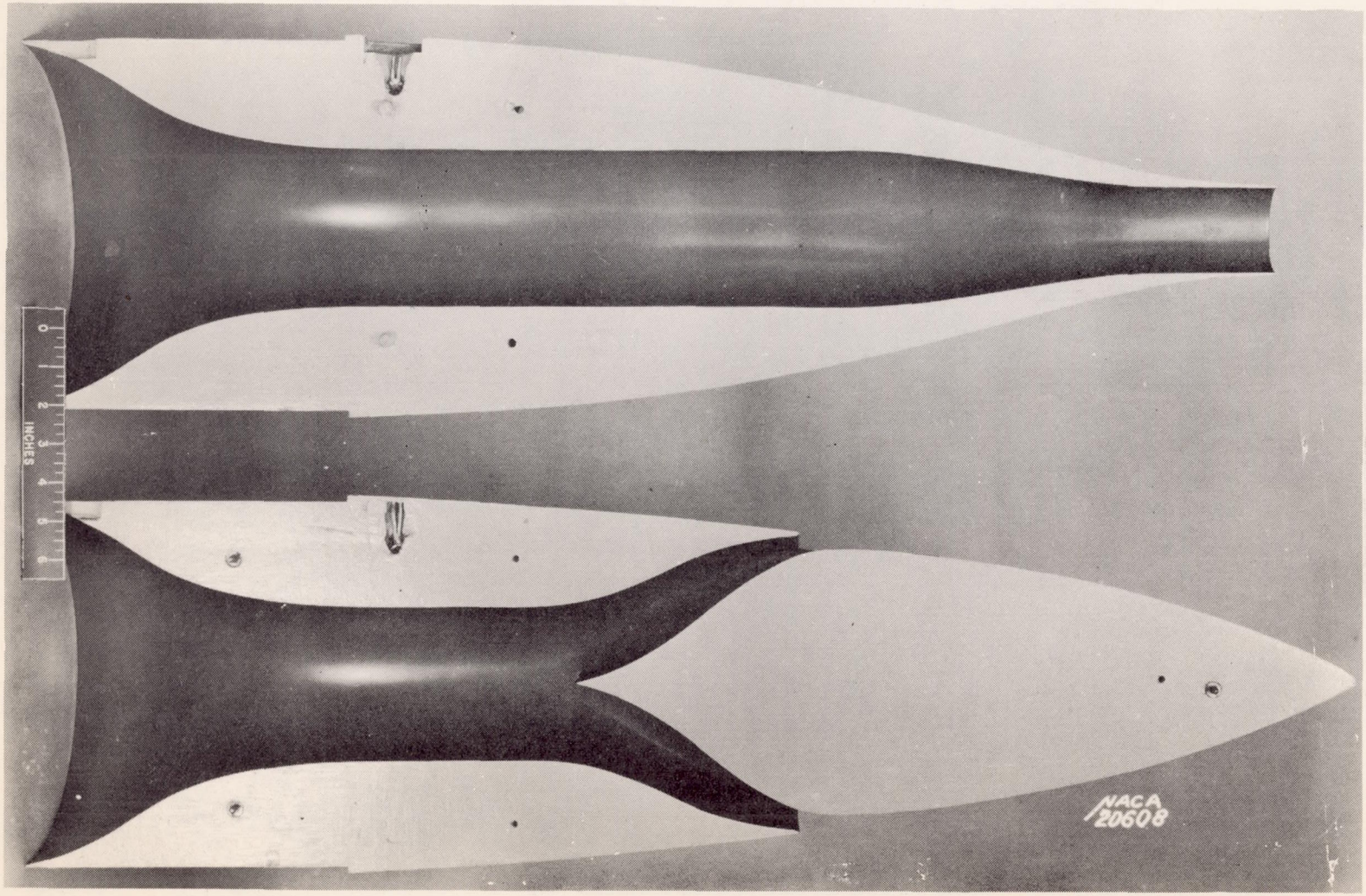

Figure 10. Comparison of internal ducts.
Tail 1-a (bottom) and tail 2-a .

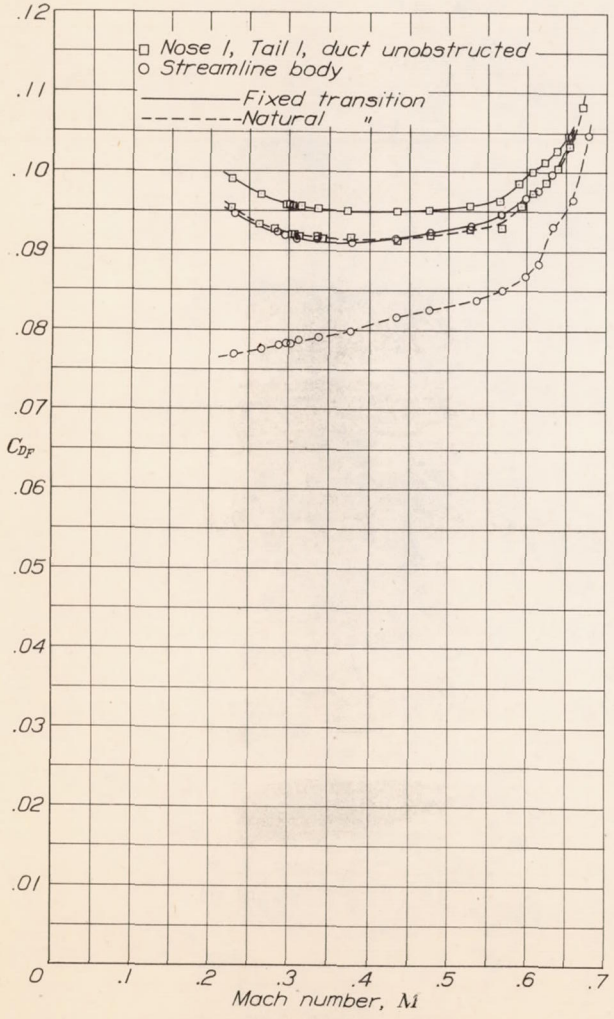

Figure 11.- Variation with Mach number of effective fuselage drag coefficients.

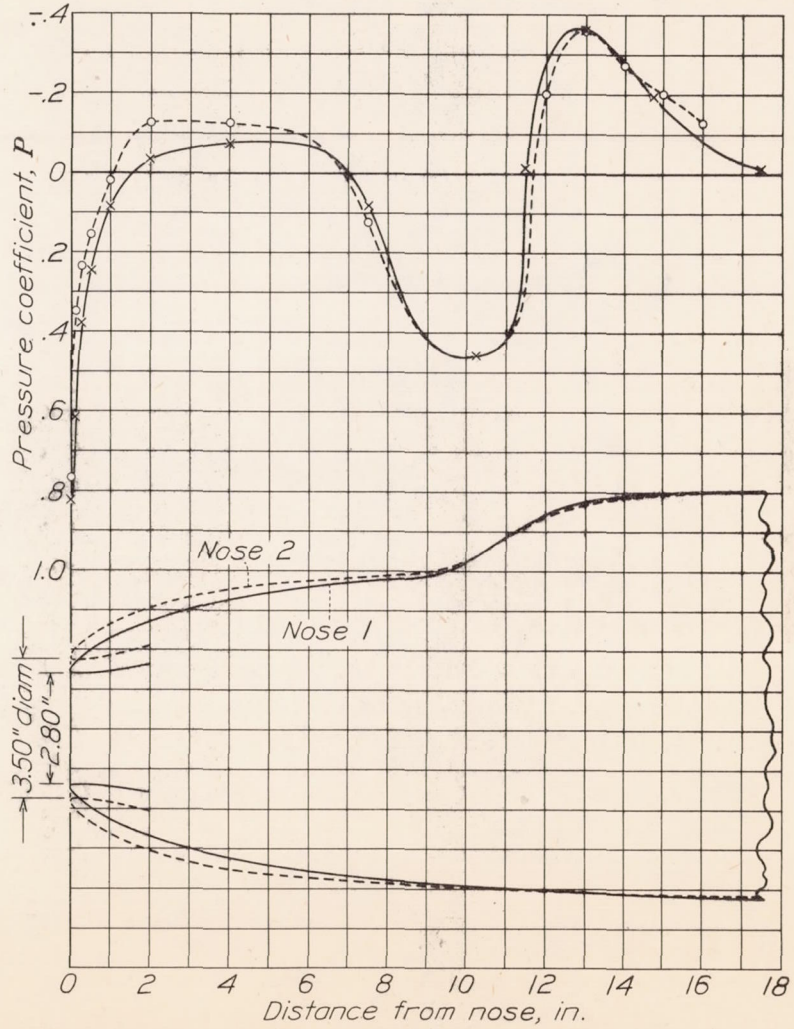

Figure 12.- Static-pressure distribution over top of noses. Q/FV=0.041.

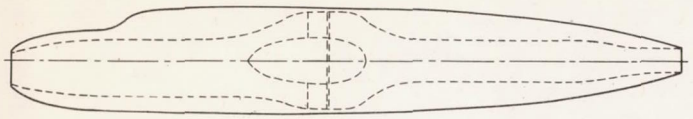

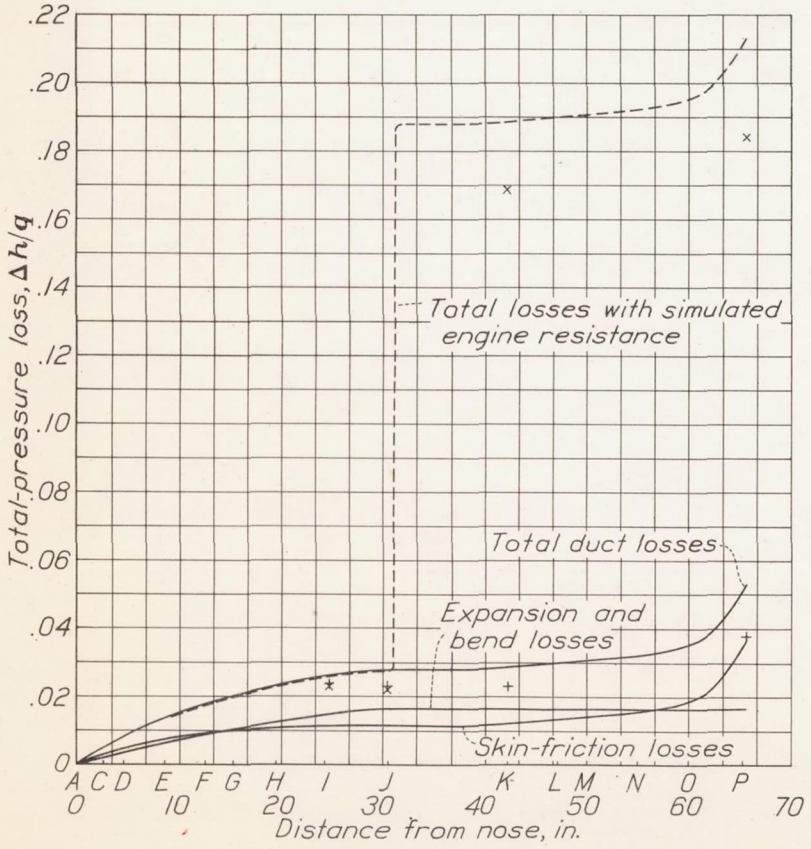

Figure 15.- Nose 2, tail 2.

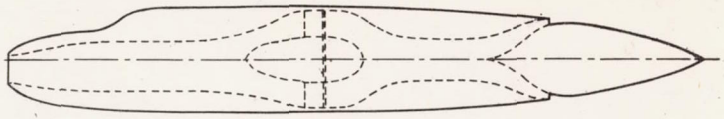

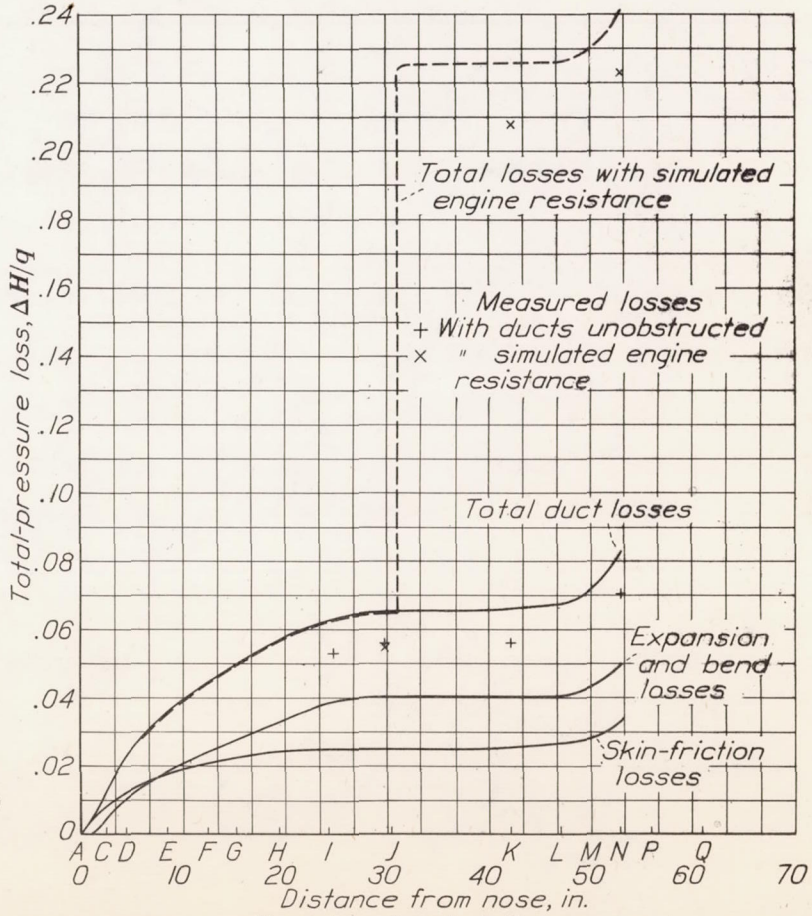

Figure 14.- Nose 1, tail 1.

Figures 14 and 15.- Analysis of duct losses and comparison of computed and measured total losses. Q/FV=0.040.